UCRL-JC-121662
PREPRINT

CONF-960738--2

Laminar Backward-Facing Step Flow using the Finite Element Method

Barbara Kornblum
Rose McCallen
Mark A. Christon
Wolfgang Kollmann

This paper was prepared for submittal to the
1996 ASME Fluids Engineering Division Summer Meeting
American Society of Mechanical Engineers, San Diego, CA
July 7-11, 1996

November 1995

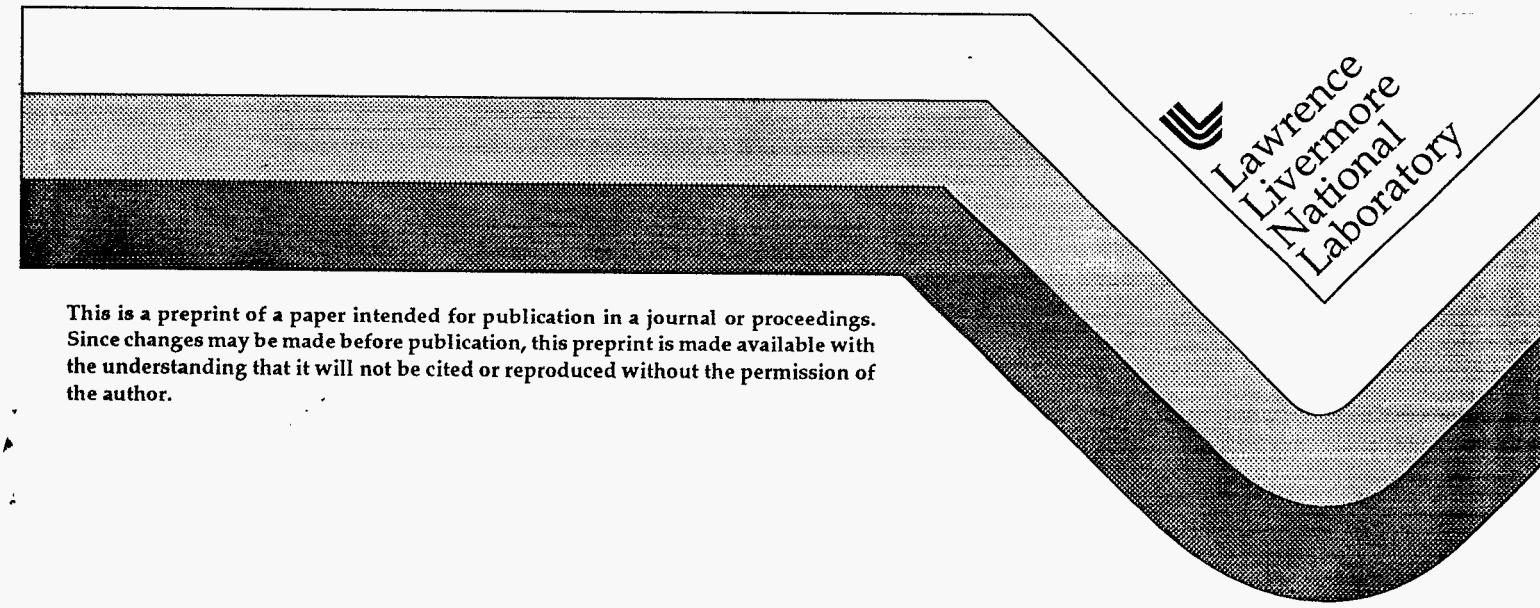

DISCLAIMER

Laminar Backward-Facing Step Flow using the Finite Element Method*

Barbara Kornblum and Rose McCallen
Lawrence Livermore National Laboratory
University of California
Livermore, California

Mark A. Christon[1]
Sandia National Laboratory
Albuquerque, New Mexico

Wolfgang Kollmann
Department of Mechanical and Aeronautical Engineering
University of California, Davis
Davis, California

ABSTRACT

Laminar, incompressible flow over a backward-facing step is calculated using a finite element spatial discretization with a piecewise continuous pressure approximation and an explicit time marching algorithm. The time-accurate evolution to steady state is demonstrated for both two-dimensional (2D) and three-dimensional (3D) simulations. This approach is shown to accurately predict the lengths of the recirculation zone on the top wall and at the step for various meshes and domain lengths, for a Reynolds number of 800 based on the average inlet velocity and twice the inlet channel height. The instantaneous and steady-state results are investigated. The steady-state solutions are evaluated by comparison to published numerical and experimental results.

* This work was performed under the auspices of the U.S. Department of Energy by Lawrence Livermore National Laboratory under Contract W-7405-Eng-48.

1. Previously at Lawrence Livermore National Laboratory.

INTRODUCTION

The finite element method (FEM) has been used by Gartling (1990) to obtain an accurate solution for *steady* 2D incompressible flow over a backward-facing step, with the intention to provide benchmark data in a format that can be used for testing and evaluation of outflow boundary conditions. However, Gartling (1990) did not investigate the effect of the outflow boundary conditions on the initial transient flow evolution, the effects of the computational channel length, or mesh grading at walls. Neither did he attempt any 3D simulations and thus, did not investigate possible out-of-plane effects. Using a spectral method, Kaiktsis et al. (1991) found 3D transient structures for laminar flow over a backward-facing step at Re = 800. Armaly et al. (1983) has published experimental data for a backward-facing step with the same expansion ratio as was modeled by Gartling (1990).

In this paper, we consider variations in the overall flow behavior due to the computational channel length in both the streamwise and cross-stream (out-of-plane) directions, as well as mesh size, mesh grading at walls, and the magnitudes of particular numerical parameters. Results indicating the separation and reattachment locations of the recirculation zones in the steady-state solution are presented for both 2D and 3D simulations. The homogeneous natural boundary conditions (zero traction), which arise directly from the FEM formulation, are applied at the exit plane, and we show the sensitivity of the flow solution to the location of this outflow boundary condition. Periodic boundary conditions were used on the lateral boundaries in the 3D simulations.

GOVERNING EQUATIONS AND NUMERICAL METHOD

In our investigation, the time-dependent incompressible Navier-Stokes equations are solved using an FEM approach. The incompressible Navier-Stokes equations are:

$$\nabla \bullet \boldsymbol{u} = 0 \tag{1}$$

$$\frac{\partial \boldsymbol{u}}{\partial t} + \boldsymbol{u} \bullet \nabla \boldsymbol{u} = -\nabla P + \upsilon \nabla^2 \boldsymbol{u} + \boldsymbol{f} \tag{2}$$

where $\boldsymbol{u} = (u_1, u_2, u_3)$ is the velocity, $P = p/\rho$ where p is the pressure and ρ is the density, υ is the kinematic viscosity, and $\boldsymbol{f}$ is the body force.

Our FEM approach is similar to that developed by Gresho et al. (1984). The computer code HYDRA (Christon 1995) is used to calculate the results presented here. Unlike the original investigations of Gresho et al. (1984), HYDRA allows for the use of unstructured

meshes with one-point integration, hourglass stabilization, and balancing tensor diffusivity (BTD) for explicit time integration.

Using the Galerkin finite element method, the discretized continuity and momentum equations can be written in matrix form as

$$C^T u = 0 \tag{3}$$

$$M_L \dot{u} + [K + A(u)]\, u + Cp = F \tag{4}$$

where u is the nodal velocity vector, p is the pressure vector, M_L is the lumped-mass matrix, K is the diffusivity, $A(u)$ is the advection operator, C is the gradient operator, and F is the user-supplied natural boundary condition. For more details see Gresho (1984) and Christon (1995).

In this study, the discrete pressure Poisson equation is solved in place of the continuity equation (3), so that continuity and momentum are decoupled and an explicit time-integration scheme is used. The discrete Poisson equation for pressure is an approximation of the continuous Poisson equation. The continuous Poisson equation is derived by taking the divergence of the momentum equation and applying the continuity equation (1). The analogous discrete Poisson equation is derived by multiplying the matrix form of the momentum equation (4) by $C^T M_L^{-1}$, and since $\frac{d}{dt}(C^T u) = 0$, we obtain

$$C^T M_L^{-1} C p = C^T M_L^{-1} (F - [K + A(u)]\, u) \tag{5}$$

where the coefficient matrix $C^T M_L^{-1} C$ is a discrete approximation of the Laplacian operator. Thus, the final discretized equations in matrix form are (4) and (5).

To reduce computational cost, a lumped mass matrix is employed and the coefficient matrices are generated using one-point Gaussian quadrature. The Q1P0 element formulation is used which provides bilinear velocity support in 2D and trilinear support in 3D with piecewise constant pressure. The pressure Poisson equation is solved directly with a parallel-vector row solver (Storaasli et al. 1990) and an explicit forward Euler time integration scheme is used for the velocity solution.

An additive correction (diffusivity) to the diffusion matrix balances the negative diffusion induced by explicit Euler time integration (i.e., balancing tensor diffusivity (BTD), Gresho et al., 1984). Also, an hour-glass correction is added to the one-point quadrature diffusion matrix to damp any zero energy modes that may be present because of the

reduced integration scheme (Goudreau and Hallquist, 1982 and Gresho et al., 1984). To reduce the computational effort in the evaluation of the advection term we use a 'centroid advection velocity' simplification as was done by Gresho et al. (1984).

PROBLEM DEFINITION

For the backward-facing step geometry, no-slip boundary conditions are imposed on the step and the upper and lower channel walls, a parabolic velocity profile is specified at the channel inlet, and zero natural boundary conditions are imposed at the channel outlet (Fig. 1). The Reynolds number (Re=UH/υ) of 800 is based on the channel height of $H = 1.0$ and the average inlet velocity of $U = (2U_{max})/3 = 1.0$ where $U_{max} = 1.5$ in a parabolic profile. Three different channel lengths, L = 12, 15, and 30, were investigated in 2D. For the 3D simulations, we considered L = 12, out-plane-width W = 1, and enforced periodic boundary conditions on the lateral boundaries (Fig. 2).

The periodic boundary conditions cause a singularity in the pressure matrix which introduces spurious pressure modes and causes the pressure results to display a checker board pattern on the upper and lower no-slip channel walls. We eliminated these modes by using a zero traction boundary condition in the x_3-direction along a single line of nodes on the bottom wall (Fig. 2). This action produces very small x_3-direction velocities, u_3, for the traction nodes on the bottom wall, but their magnitude is machine zero and thus, the no-slip condition is satisfied.

RESULTS

We report numerical results for our 2D and 3D investigations in tabular form to enable precise comparisons. Contour pictures are included for qualitative evaluation. Time evolution of the flow is demonstrated with time-histories plots. Our video tape with animations of both 2D and 3D time-accurate simulations is complete and will be shown during our July 1996 presentation.

Convergence and Comparison Criteria

We used the points where the flow separates and reattaches for comparison in our parameter studies. These separation and reattachment points define the lengths of recirculation zones on the top and bottom walls. The distance l_1 is the length of the major recirculation zone on the bottom wall measured from the step. The lengths l_2 and l_3 are the

separation and reattachment positions on the top wall. We determined these lengths by examining the vorticity along the upper and lower walls of the channel. The flow separates or reattaches where the shear stress is zero and for 2D results the vorticity is zero when the shear stress is zero. We found the locations of zero vorticity by interpolating between grid points where the vorticity changed sign. This technique also applied when analyzing our 3D cases because the results were perfectly 2D.

Spatial convergence of our solutions is demonstrated from consistent separation and reattachment positions calculated with various mesh sizes. As the mesh was refined, the amount of change in the solution diminished. The converged solutions also exhibit smooth velocity profiles in high velocity gradient regions.

Temporal convergence was determined by examining time-histories of velocity at several point locations in the flow. In addition, the invariance of the flow's total kinetic energy $KE = \boldsymbol{u}^T \boldsymbol{M}_L \boldsymbol{u}$ demonstrates a time-converged solution by evaluation of a global quantity. A steady solution is achieved well before the simulation time of 400, which is the point in time that we chose to evaluate l_1, l_2, and l_3.

Steady-State Solution

Our 2D and 3D simulations evolve to a steady-state solution for Reynolds number of 800 (Fig. 3, 4, and 5), contrary to the results of Kaiktsis et al. (1991), who was not able to obtain a steady solution in 2D or 3D at this Reynolds number. Our 3D simulation results are identical to our 2D results. They converge to a steady solution which does not exhibit 3D structures. Figure 6 shows the time history of the global kinetic energy which helps demonstrate time convergence. Local velocity time histories (Fig. 7 and 8) at selected point locations also show that time convergence to a steady state has been well achieved.

The streamfunction contours in Fig. 3 and the pressure contours in Fig. 4 capture the well-known character of the backward-facing step for the steady-state 2D solution. Results of 3D simulations are more difficult to display without the use of color. We have chosen isosurfaces of pressure to demonstrate the steady-state 3D solution in black and white (Fig. 5) because isosurfaces of the quantities vorticity or velocity would overlap and prevent details from being seen.[1] It is clear that the 3D pressure isosurfaces of Fig. 5 have no variation in the x_3 direction and are identical to the 2D results in Fig. 4.

1. We will use color pictures and animation during our presentation.

We were able to shorten the channel length by a significant amount which reduced the size of the computational domain and thus the resources required to obtain a good solution. In Table 1, solutions are compared for three different channel lengths having the same uniform element size. These solutions are essentially identical because the results vary by less than one element size. The positions of the steady-state recirculation zones are relatively insensitive to the channel lengths studied here. This result reflects the ability of the homogeneous natural boundary condition to capture the steady-state outflow condition.

In Table 2, we compare our solutions for a channel length of 12, with different field discretizations including selected results from our investigation of graded meshes and out-of-plane 3D effects. Our only attempt to optimize the distribution of the elements in the graded meshes was to use the simple rule of grading finer in wall regions. We found very little change in the solution until we moved to meshes with coarse x_1 discretization. Results for our coarsest mesh (Case H) are only 3% different from our finest mesh (Case C) even though the finest has 18 times more elements. We found no difference in the solutions in going from 2D to 3D and keeping the same mesh in the $x_1 \times x_2$ plane, and we found no variation in the 3D results for different x_3-direction mesh sizes.

Generally, the calculated lengths l_1, l_2, and l_3 are in good agreement with Gartling (1990), even though Gartling used higher order approximations (9 node elements) than that used in our approach (4 node elements in 2D). Experimental results from Armaly et al. (1983) were estimated from figures in the paper and are included in Table 2. As other investigators have found, numerical simulations do not exactly agree with experiment.

The solution was not affected by the chosen time step size, as long as the time step remained below the Courant limit. This also means that the solution was insensitive to BTD because BTD is proportional to time step size. The test that was performed to evaluate the influence of time step on the solution involved decreasing the time step by factors of 1.5 and 3 on our finest mesh (Case A) and applying our steady-state spatial convergence criteria. In addition, we found no effect on the reattachment positions for a factor of ten variation in the hourglass coefficient.

Transient Phenomena

Our investigation of the flow evolution exhibits a transient pressure fluctuation when the initial vortex reaches the exit of the computational domain at L = 12. The exiting vortex causes an abrupt change in the outlet flow, and the outflow boundary conditions must

quickly adjust from what is essentially a zero pressure condition at the exit plane to the low pressure vortex so that the homogeneous natural boundary condition is satisfied. The pressure fluctuation lasts approximately 10 time units. It affects the entire flow field instantaneously, because of the effective infinite sound speed for incompressible flow. This feature, which is purely a computational phenomenon, is clearly seen in our 2D and 3D animations of pressure results.

Computational Resources

All of the cases documented in this report were run on a Silicon Graphics Power Indigo 2 Workstation using the parallel-vector row solver (Storaasli et al. 1990) for the pressure Poisson equation in HYDRA (Christon 1995). Table 3 summarizes the computational resources required to run each case. Memory requirements are dominated by the pressure Poisson equation and correlate with the matrix half-bandwidth. The element cycle time represents the number of microseconds (μsec) required to advance the solution of one element through one time step. Total run time is the CPU time necessary to compute the steady-state solution at time = 400.

There is a strong correlation between total storage (memory) required and matrix bandwidth, with additional storage requirements based on number of elements. As the element count and bandwidth decreased, so did memory. There also exists an obvious correlation between the element cycle time and the bandwidth. Cases A, B, and C have the same bandwidth and virtually identical cycle times. The total run time for these cases, however, is proportional to the element count.

We have included this information to demonstrate the significant reduction in resources that was achieved by cutting the domain from L = 30 to L = 12, and in using coarser, graded meshes.

CONCLUSIONS

The finite element method with a piecewise continuous pressure approximation and an explicit time marching algorithm accurately solves the backward-facing step problem at a Reynolds number of 800. Using homogeneous natural boundary conditions allows for a significant reduction in the length of the computational domain and grading at the walls reduces the overall mesh size. These factors contribute to a reduction in the resources required to obtain converged results.

Both 2D and 3D simulations evolve to the same steady-state solution with the 3D simulation exhibiting no 3D structures. Although the periodic boundary conditions used in the 3D simulations can cause pressure modes, we eliminated them by the use of zero traction boundary conditions in the out-of-plane direction along the center line of the bottom wall.

During the flow evolution, a pertubation in the pressure solution occurs when the initial vortex exits the computational domain. This is due to the abrupt imposition of a strong vortex on the outflow homogeneous natural boundary condition.

This benchmark problem also provided an excellent opportunity to demonstrate the ability of state-of-the-art workstations to solve problems that were formerly relegated to main frame computers.

Acknowledgment

We are grateful to Michael Loomis from the Computations Department at LLNL for creating the 2D and 3D flow animations.

References

Armaly, B.F., Durst, F., Pereira, J.C.F., Schonug, B. 1983, "Experimental and Theoretical Investigation of Backward Facing Step Flow", *Journal of Fluid Mechanics*, Vol. 127, pp. 473-496.

Christon, M., 1995, "HYDRA: A Finite Element Computational Fluid Dynamics Code," LLNL document UCRL-MA-121344.

Gartling, D.K., 1990, "A Test Problem for Outflow Boundary Conditions - Flow Over a Backward-Facing Step," *International Journal for Numerical Methods in Fluids*, Vol. 11, pp. 953-967.

Goudreau, G.L. and Hallquist, J.O., 1982, "Recent Developments in Large-Scale Finite Element Lagrangian Hydrocode Technology," *Computational Methods in Applied Mechanics and Engineering*, Vol. 33, pp. 725.

Gresho, P.M., Chan, S.T., Lee, R.L., and Upson, C.D., 1984, "A Modified Finite Element Method for Solving the Time-Dependent, Incompressible Navier-Stokes Equations. Part1: Theory," *International Journal for Numerical Methods in Fluids*, Vol. 4, pp. 557-598.

Kaiktsis, L., Karniadakis, G., and Orszag, S.A., "Onset of Three-Dimensionality, Equilibria, and Early Transition in Flow over a Backward-Facing Step," *Journal of Fluid Mechanics*, Vol. 231, pp. 501-528.

Storaasli, O.O., D.T. Nguyen, T.K. Agaruwal, "A Parallel-Vector Algorithm for Rapid Structural Analysis on High-Performance Computers," NASA Technical Memorandum 102614, April, 1990.

TABLE 1. Comparison of 2D results for three different channel lengths using uniform element size $\Delta x_1 = \Delta x_2 = 0.0125$.

run no.	Channel Length, L	element count	l_1	l_2	l_3
A	30	128,000 *	6.03	4.90	10.37
B	15	96,000	6.03	4.90	10.37
C	12	76,800	6.03	4.91	10.35

* mesh was uniform for $0 < x_1 < 15$, then graded 1:2 for $15 < x_1 < 30$ as in Gartling (1990).

TABLE 2. Comparison of results for 2D and 3D simulations with channel length of 12.

run no.	run dim.	Δx_1 min.	Δx_1 max.	Δx_2 min.	Δx_2 max	Δx_3	x_1 mesh	x_2 mesh	x_3 mesh	element count	l_1	l_2	l_3
C	2D	.0125	n/a	.0125	n/a	n/a	960	80	n/a	76,800	6.03	4.91	10.35
D	2D	.0167	n/a	.0167	n/a	n/a	720	60	n/a	43,200	5.99	4.91	10.31
E	2D	.0250	n/a	.0250	n/a	n/a	480	40	n/a	19,200	5.90	4.91	10.22
F	2D	.0125	.025	.0125	.0250	n/a	482	44	n/a	21,208	5.94	4.82	10.32
G	2D	.0250	.050	.0250	.0417	n/a	340	32	n/a	10,880	5.80	4.82	10.18
H	2D	.0167	.178	.0208	.0417	n/a	124	34	n/a	4,216	5.83	4.76	10.21
I	3D	.0167	.178	.0209	.0417	.167	124	34	6	25,296	5.83	4.76	10.21
J	3D	.0167	.178	.0209	.0417	.100	124	34	10	42,160	5.85	4.76	10.21
Gartling (1990): L=30 with 32,000 9-node elements											6.10	4.85	10.48
Armaly et al. (1983): we estimated these results from figures in the paper											7.0	5.3	9.4

TABLE 3. Use of Computational Resources

run no.	run dim.	element count	memory (MWords)	1/2 Band Width	elem. cycle time (μ sec)	total run time(hrs.)
A	2D	128,000	16.87	82	27.5	54.
B	2D	96,000	12.65	82	26.6	40.
C	2D	76,000	10.12	82	26.4	32.
D	2D	43,200	4.84	62	21.8	15.
E	2D	19,200	1.77	42	16.1	4.8
F	2D	21,208	2.04	46	17.2	5.7
G	2D	10,880	0.92	34	13.0	2.2
H	2D	4,216	0.36	36	8.5	0.6
I	3D	25,296	7.21	215	69.1	26.
J	3D	42,160	17.82	359	94.2	61.

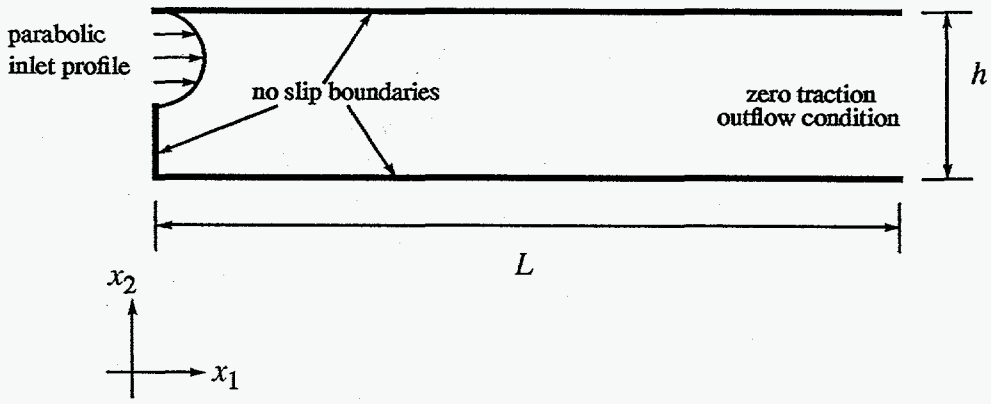

FIG. 1. PROBLEM DEFINITION FOR 2D BACKWARD-FACING STEP.

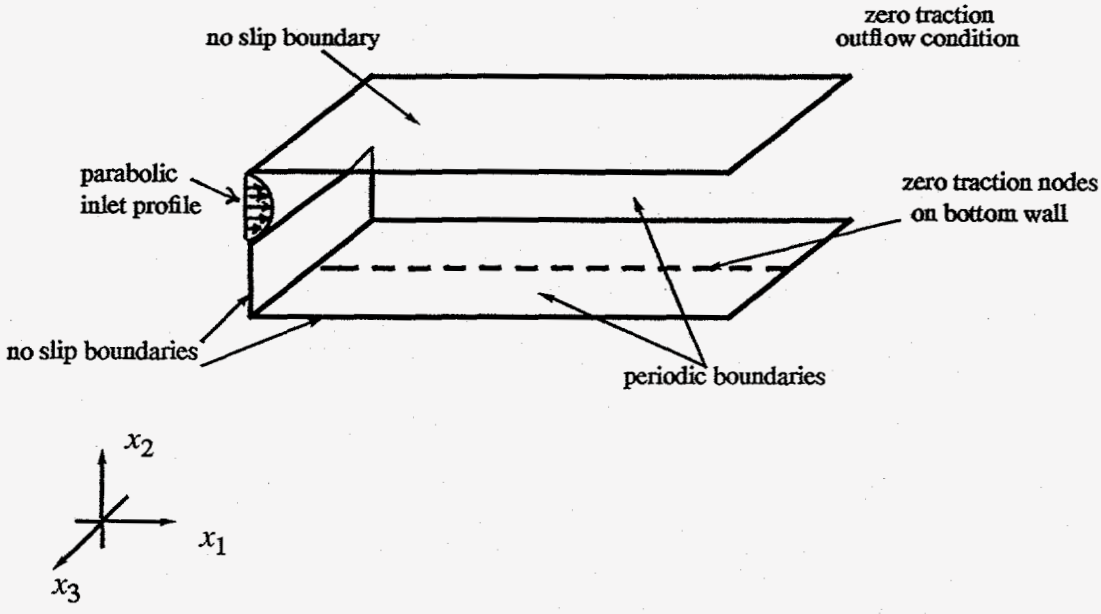

FIG. 2. PROBLEM DEFINITION FOR 3D BACKWARD-FACING STEP.

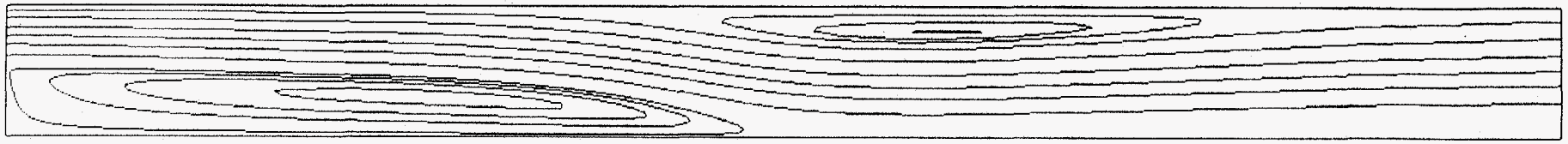

Figure 3. Streamfunction contours for 2D steady-state solution in channel length 12.

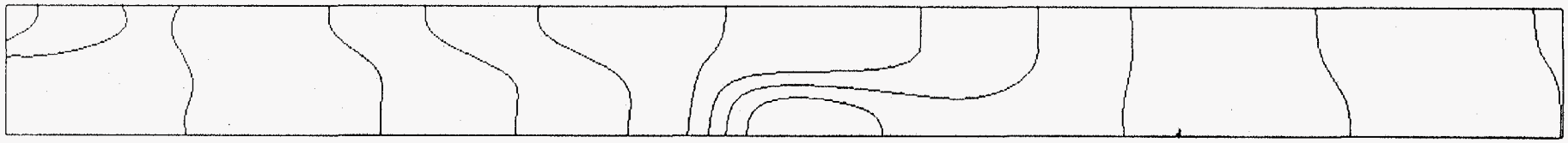

Figure 4. Pressure contours for 2D steady-state solution in channel length 12.

Figure 5. Pressure isosurfaces for 3D steady-state solution in channel length 12.

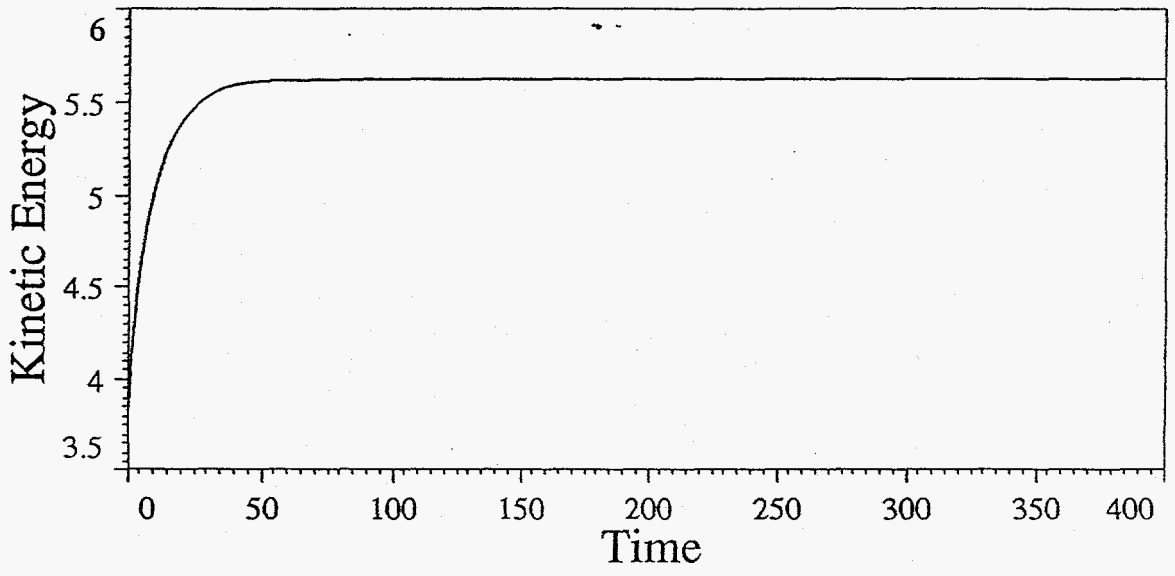

Figure 6. **Total kinetic energy of the flow taken from results for Case A.**

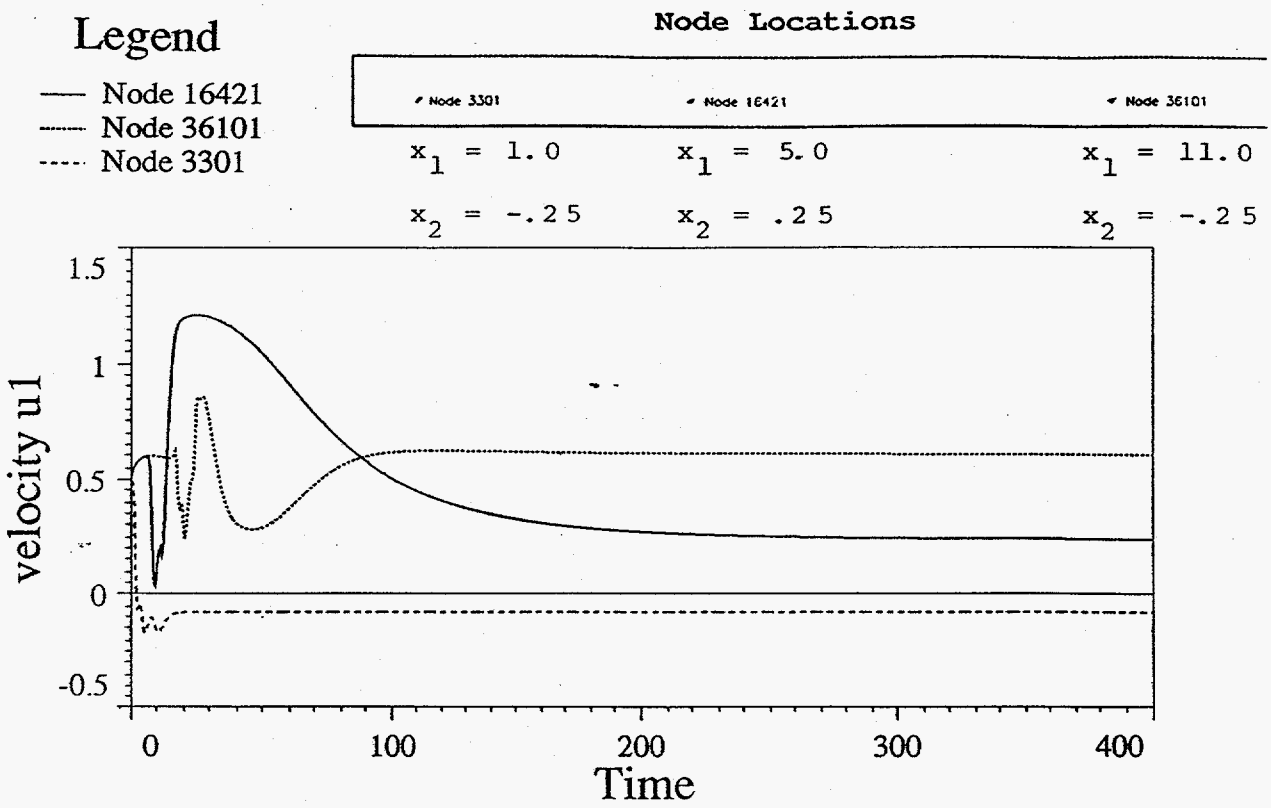

Figure 7. Time history of velocity u1 for selected nodes

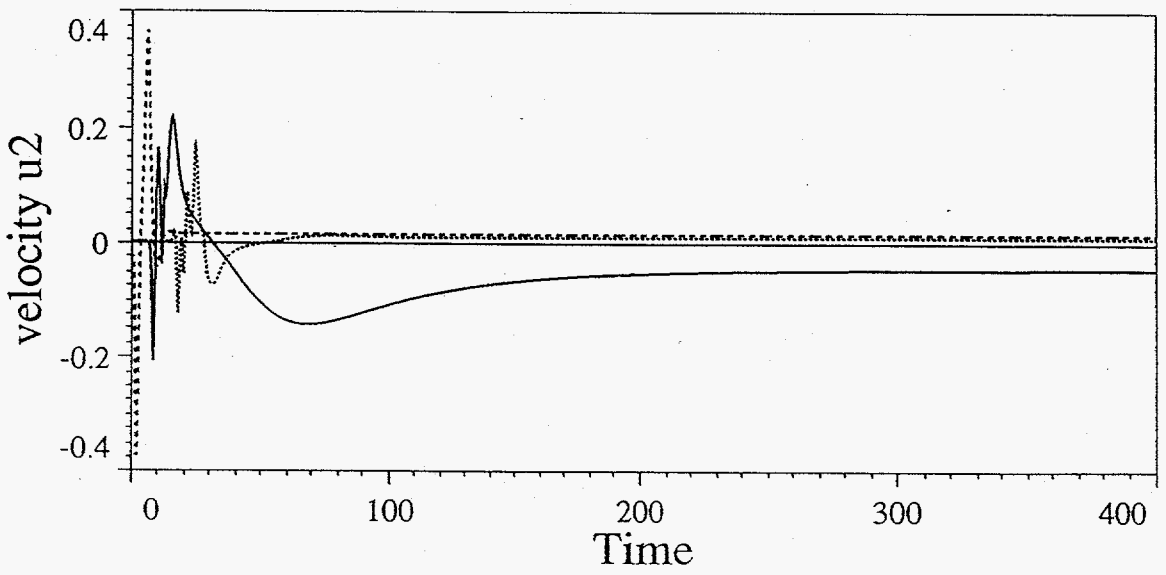

Figure 8. Time history of velocity u2 for selected nodes